Weierstraß-Institut
für Angewandte Analysis und Stochastik

im Forschungsverbund Berlin e.V.

Preprint ISSN 0946 – 8633

Simulation of microwave and semiconductor laser structures including PML: Computation of the eigen mode problem, the boundary value problem, and the scattering matrix

Georg Hebermehl[1], Jürgen Schefter[1], Rainer Schlundt[1],

Thorsten Tischler[2], Horst Zscheile[2], Wolfgang Heinrich[2]

submitted: 14th November 2005

[1] Weierstrass Institute for Applied Analysis and Stochastics
Mohrenstraße 39
10117 Berlin, Germany
E-Mail: hebermehl@wias-berlin.de
schlundt@wias-berlin.de

[2] Ferdinand-Braun-Institut für Höchstfrequenztechnik
Gustav-Kirchhoff-Str. 4
12489 Berlin, Germany
E-Mail: w.heinrich@ieee.org

No. 1067
Berlin 2005

2000 *Mathematics Subject Classification.* 35Q60, 65N22, 65F15, 65F10, 78M25.

Key words and phrases. Microwave device, Semiconductor laser, Simulation, Maxwell's equations, Scattering matrix, Boundary value problem, PML boundary condition, Eigenvalue problem, Linear algebraic equations, Rectangular grids, Tetrahedral nets.

Edited by
Weierstraß-Institut für Angewandte Analysis und Stochastik (WIAS)
Mohrenstraße 39
10117 Berlin
Germany

Fax: + 49 30 2044975
E-Mail: preprint@wias-berlin.de
World Wide Web: http://www.wias-berlin.de/

Abstract

The properties of microwave circuits and optical structures can be described in terms of their scattering matrix which is extracted from the orthogonal decomposition of the electric field. We discretize the Maxwell's equations with orthogonal grids using the Finite Integration Technique (FIT). Maxwellian grid equations are formulated for staggered nonequidistant rectangular grids and for tetrahedral nets with corresponding dual Voronoi cells. The surface of the computation domain is assumed to be an electric or a magnetic wall, open-region problems require uniaxial Perfectly Matched Layer (PML) absorbing boundary conditions. Calculating the excitations at the ports, one obtains eigenvalue problems and then large-scale systems of linear algebraic equations. This paper is a revised version of the preprint no. 987.

Contents

List of Figures

1 Introduction

Today, electromagnetic simulation forms an indispensable part in the development of microwave circuits as well as in diode laser design. Since the simulation methods are computationally too expensive to handle complete microwave circuits, analysis has to concentrate on critical parts, such as transmission-line discontinuities and junctions. These elements can be represented by the basic description shown in Fig. 1: a structure of arbitrary geometry which is connected to the remaining circuit by transmission lines. The passive structure (e.g. coplanar waveguide, coupled spiral inductors, via hole, impedance step) forms the central part of the problem. Short transmission line sections are attached to it in order to describe its interaction with other circuit elements.

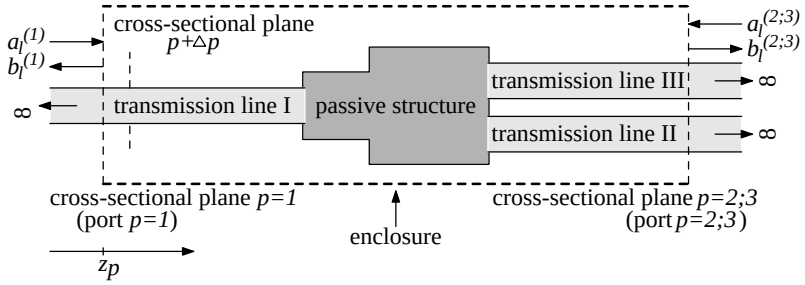

Figure 1: The basic structure under investigation

2 Scattering Matrix

The aim consists in the computation of the scattering matrix, which describes the structure in terms of the wave modes on the transmission line sections at the ports. The wave-mode quantities are derived by assuming the transmission-line sections to be infinitely long and longitudinally homogeneous. The generalized scattering matrix is defined as follows:

$$S = (S_{\rho,\sigma}),\ \ \rho,\sigma = 1(1)m_s, \quad \text{with} \quad m_s = \sum_{p=1}^{\overline{p}} m^{(p)},\ \ \rho = l + \sum_{q=1}^{p-1} m^{(q)}. \qquad (1)$$

$m^{(p)}$ denotes the number of modes which have to be taken into account at the port p. $\overline{p}$ is the number of ports. The modes on a port p are numbered with l, $l = 1(1)m^{(p)}$.

That means, the dimension m_s of this matrix is determined by the total number of modes at all ports.

The computation of the scattering matrix is outlined as follows.
The scattering matrix can be extracted from the orthogonal decomposition of the electric field into a sum of mode fields [4]. This has to be done at a pair of neighboring cross-sectional planes z_p and $z_{p+\Delta p}$ on each waveguide for a number of linearly independent excitations. The electric fields at the planes z_p and $z_{p+\Delta p}$ are calculated solving an eigenvalue problem for the infinitely long waveguide (see section 5) and a boundary value problem for the 3D structure (see section 3), respectively.

The computation of the scattering matrix is based on the orthogonality relation for the electric and magnetic fields of different modes

$$\int_{\Omega} (\vec{E}_{t,l}(z) \times \vec{H}_{t,m}(z)) \cdot d\vec{\Omega} = \eta_m \delta_{l,m}, \tag{2}$$

where $\delta_{l,m}$ is the Kronecker symbol. $\vec{H}_{t,m}$ denotes the transverse magnetic mode fields.

In the case of degenerate modes, i.e., the algebraic multiplicity of the corresponding eigenvalues is larger than unity, we have to use first (2) in order to orthogonalize the modes (see [9]).

For sake of simplicity we assume the cross section is located on the left-handed (x, y)-plane of the enclosure (see Fig. 1). We consider all exciting modes with amplitudes a_l in positive z-direction and all outgoing modes with amplitudes b_l in negative z-direction. Then the transverse mode field at a cross-sectional plane z is given by

$$\vec{E}_t(z) = \sum_{l=1}^{m^{(p)}} a_l \vec{E}_{t,l} e^{-\jmath k_{z_l} z} + \sum_{l=1}^{m^{(p)}} b_l \vec{E}_{t,l} e^{+\jmath k_{z_l} z} = \sum_{l=1}^{m^{(p)}} w_l(z) \vec{E}_{t,l} \tag{3}$$

with

$$w_l(z) = a_l e^{-\jmath k_{z_l} z} + b_l e^{+\jmath k_{z_l} z} = \tilde{a}_l(z) + \tilde{b}_l(z), \tag{4}$$

where k_{z_l} is the propagation constant. The application of (3) with (4) at a pair of neighboring cross-sectional planes z_p and $z_{p+\Delta p}$ gives because of $\vec{H}_{t,m}(z_{p+\Delta p}) = \vec{H}_{t,m}(z_p)$:

$$\begin{aligned} \frac{1}{\eta_m} \int_{\Omega} (\vec{E}_t(z_p) \times \vec{H}_{t,m}(z_p) \cdot d\vec{\Omega} &= \tilde{a}_m^{(p)} + \tilde{b}_m^{(p)} &= w_m^{(p)}, \\ \frac{1}{\eta_m} \int_{\Omega} (\vec{E}_t(z_{p+\Delta p}) \times \vec{H}_{t,m}(z_p) \cdot d\vec{\Omega} &= \tilde{a}_m^{(p+\Delta p)} + \tilde{b}_m^{(p+\Delta p)} &= w_m^{(p+\Delta p)}. \end{aligned} \tag{5}$$

We get $\vec{E}_t(z_p)$ solving eigenvalue problems for the transmission lines (see section 5). $\vec{H}_{t,m}(z_p)$ can be computed from the known electric field $\vec{E}_{t,m}$ of mode m (see [9]).

The values of the weighted mode amplitude sums $w_m^{(p)}$ are given (see the discussion to follow). Thus, the normalization constant η_m can be computed by evaluating the orthogonality relation in the first equation of (5). $\vec{E}_t(z_{p+\Delta p})$ is computed solving boundary value problems for the discontinuity (see section 3). Thus, the weighted mode amplitude sums $w_m^{(p+\Delta p)}$ can be calculated by using the second equation of (5).

By using (see (4))

$$\tilde{a}_m^{(p+\Delta p)} = \tilde{a}_m^{(p)} e^{-\jmath k_{z_l}^{(p)} \Delta z_p}, \quad \tilde{b}_m^{(p+\Delta p)} = \tilde{b}_m^{(p)} e^{+\jmath k_{z_l}^{(p)} \Delta z_p}, \tag{6}$$

we eliminate $\tilde{a}_m^{(p+\Delta p)}$ and $\tilde{b}_m^{(p+\Delta p)}$ in (5), and obtain

$$\tilde{a}_m^{(p)} = \frac{w_m^{(p)} e^{+\jmath k_{z_m}^{(p)} \Delta z_p} - w_m^{(p+\Delta p)}}{e^{+\jmath k_{z_m}^{(p)} \Delta z_p} - e^{-\jmath k_{z_m}^{(p)} \Delta z_p}} \quad , \quad \tilde{b}_m^{(p)} = \frac{w_m^{(p+\Delta p)} - w_m^{(p)} e^{-\jmath k_{z_m}^{(p)} \Delta z_p}}{e^{+\jmath k_{z_m}^{(p)} \Delta z_p} - e^{-\jmath k_{z_m}^{(p)} \Delta z_p}} \quad . \tag{7}$$

By using (7) reflection coefficients

$$r_m^{(p)} = \frac{\tilde{b}_m^{(p)}}{\tilde{a}_m^{(p)}} = \frac{e^{-\jmath k_{z_m}^{(p)} \Delta z_p} - \frac{w_m^{(p+\Delta p)}}{w_m^{(p)}}}{\frac{w_m^{(p+\Delta p)}}{w_m^{(p)}} - e^{+\jmath k_{z_m}^{(p)} \Delta z_p}} \tag{8}$$

are computed for all modes $\rho = 1(1)m_s$ and all excitations $\nu = 1(1)m_s$.

The values $w_m^{(p)}$ are given, and than we form the vectors

$$\vec{\bar{w}}_\nu = (\bar{w}_{1,\nu}, \ldots, \bar{w}_{\rho,\nu}, \ldots, \bar{w}_{m_s,\nu})^T, \quad \nu = 1(1)m_s. \tag{9}$$

The vectors (9) have to be linear independent. That is achieved here by choosing the components of $\vec{\bar{w}}_\nu$ in the following way:

$$\bar{w}_{\rho,\nu} = \begin{cases} |w_m^{(p)}| & \text{for} \quad 1 \le \rho \le m_s + 1 - \nu \\ -|w_m^{(p)}| & \text{for} \quad m_s + 2 - \nu \le \rho \le m_s \end{cases} \quad , \quad \rho = m + \sum_{q=1}^{p-1} m^{(q)}, \tag{10}$$

with

$$w_m^{(p)} = 1.0, \quad m = 1(1)m^{(p)}, \quad p = 1(1)\overline{p}. \tag{11}$$

With this choice of $\vec{\bar{w}}_\nu$ (see (9), (10), and (11)) the vectors $\vec{\bar{r}}_\nu$, $\vec{\bar{a}}_\nu$ and $\vec{\bar{b}}_\nu$ are built up analogously (see (7) and (8)):

$$\begin{array}{rclrcl} \vec{\bar{r}}_\nu & = & (\bar{r}_{1,\nu}, \ldots, \bar{r}_{\rho,\nu}, \ldots, \bar{r}_{m_s,\nu})^T, & \bar{r}_{\rho,\nu} & = & r_m^{(p)}, \\ \vec{\bar{a}}_\nu & = & (\bar{a}_{1,\nu}, \ldots, \bar{a}_{\rho,\nu}, \ldots, \bar{a}_{m_s,\nu})^T, & \bar{a}_{\rho,\nu} & = & \tilde{a}_m^{(p)}, \\ \vec{\bar{b}}_\nu & = & (\bar{b}_{1,\nu}, \ldots, \bar{b}_{\rho,\nu}, \ldots, \bar{b}_{m_s,\nu})^T, & \bar{b}_{\rho,\nu} & = & \tilde{b}_m^{(p)}. \end{array} \tag{12}$$

The relation between (ρ, ν) on the one hand and $(m, (p))$ on the other hand is given by (10) and (11). The choice of $\vec{\bar{w}}_\nu$ and the relations between the indices are demonstrated by a small example in [9].

That means, we have to solve m_s boundary value problems with the boundary conditions (see sections 3 and 6)

$$\vec{E}_{t,\nu} = \sum_{\rho=1}^{m_s} \bar{w}_{\rho,\nu} \vec{E}_{t,l}(z_p), \quad \rho = l + \sum_{q=1}^{p-1} m^{(q)}, \quad p = 1(1)\overline{p}, \quad \nu = 1(1)m_s, \tag{13}$$

in order to compute $w_m^{(p+\Delta p)}$.

The scattering matrix S (see (1)) is defined by

$$\vec{\bar{b}}_\nu = S\vec{\bar{a}}_\nu, \quad \nu = 1(1)m_s, \tag{14}$$

or (see (12))

$$\bar{b}_{\rho,\nu} = \sum_{\sigma=1}^{m_s} S_{\rho,\sigma} \cdot \bar{a}_{\sigma,\nu}, \quad \rho,\nu = 1(1)m_s. \tag{15}$$

Because of (5) and (8) we have

$$\begin{array}{lcl} \bar{w}_{\rho,\nu} & = & \bar{a}_{\rho,\nu} + \bar{b}_{\rho,\nu}\,, \\ 0 & = & \bar{r}_{\rho,\nu}\bar{a}_{\rho,\nu} - \bar{b}_{\rho,\nu}, \end{array} \quad \text{or} \quad \begin{array}{lcl} \bar{a}_{\rho,\nu}(1+\bar{r}_{\rho,\nu}) & = & \bar{w}_{\rho,\nu}, \\ \bar{b}_{\rho,\nu}(1+\bar{r}_{\rho,\nu}) & = & \bar{r}_{\rho,\nu}\bar{w}_{\rho,\nu}, \end{array} \quad \rho,\nu = 1(1)m_s. \tag{16}$$

Multiplying Eq. (15) with the product $\prod_{\mu=1}^{m_s}(1+\bar{r}_{\mu,\nu})$ gives

$$\bar{b}_{\rho,\nu} \prod_{\mu=1}^{m_s}(1+\bar{r}_{\mu,\nu}) = \sum_{\sigma=1}^{m_s} S_{\rho,\sigma}\bar{a}_{\sigma,\nu} \prod_{\mu=1}^{m_s}(1+\bar{r}_{\mu,\nu}), \quad \rho,\nu = 1(1)m_s. \tag{17}$$

Substitution of (16) into the relation (17) gives

$$R_{\rho,\nu} = \sum_{\sigma=1}^{m_s} S_{\rho,\sigma} W_{\sigma,\nu} \quad \text{or} \quad R = SW \tag{18}$$

with

$$W_{\rho,\nu} = \bar{w}_{\rho,\nu} \prod_{\mu=1,\mu\neq\rho}^{m_s} (1+\bar{r}_{\mu,\nu}), \quad R_{\rho,\nu} = \bar{r}_{\rho,\nu} W_{\rho,\nu}. \tag{19}$$

That means, we have to solve m_s linear algebraic equations in order to compute the $(m_s)^2$ coefficients of S:

$$W^T(S_{\rho,1},\ldots,S_{\rho,m_s})^T = (R_{\rho,1},\ldots,R_{\rho,m_s})^T, \quad \rho = 1(1)m_s. \tag{20}$$

3 Boundary Value Problem

A three-dimensional boundary value problem can be formulated using the integral form of Maxwell's equations in the frequency domain [1] in order to compute the electromagnetic field within the structure of interest:

$$\oint_{\partial\Omega} \vec{H}\cdot d\vec{s} = \int_\Omega \jmath\omega[\epsilon]\vec{E}\cdot d\vec{\Omega}, \qquad \oint_{\cup\Omega} ([\epsilon]\vec{E})\cdot d\vec{\Omega} = 0, \tag{21}$$

$$\oint_{\partial\Omega} \vec{E}\cdot d\vec{s} = -\int_\Omega \jmath\omega[\mu]\vec{H}\cdot d\vec{\Omega}, \qquad \oint_{\cup\Omega} ([\mu]\vec{H})\cdot d\vec{\Omega} = 0, \tag{22}$$

$$\vec{D} = [\epsilon]\vec{E}, \quad \vec{B} = [\mu]\vec{H}. \tag{23}$$

The electric and magnetic flux densities $\vec{D}$ and $\vec{B}$ are complex functions of the spatial coordinates. $\omega = 2\pi f$ is the angular frequency of the sinusoidal excitation, and $\jmath^2 = -1$. f denotes the frequency. In the left-hand sides of formulae (21) and (22) Ω is an open surface surrounded by a closed contour $\partial\Omega$. The direction of the element $d\vec{s}$ of the contour $\partial\Omega$ is determined according to a right-hand system. In the right-hand sides of (21) and (22) $\cup\Omega$ is a closed surface with an interior volume. The complex electric permittivity $[\epsilon]$ and the magnetic permeability $[\mu]$ are diagonal tensors.

At the ports p the transverse electric field $\vec{E}_t(z_p)$ is given by superposing weighted transmission line modes $\vec{E}_{t,l}(z_p)$ (see (3)):

$$\vec{E}_t(z_p) = \sum_{l=1}^{m^{(p)}} w_l(z_p)\vec{E}_{t,l}(z_p). \tag{24}$$

The transverse electric mode fields have to be computed solving an eigenvalue problem for the transmission lines (see section 5). All other parts of the surface of the computation domain are assumed to be an electric or a magnetic wall:

$$\vec{E} \times \vec{n} = 0 \quad \text{or} \quad \vec{H} \times \vec{n} = 0. \tag{25}$$

The simulation of open-region problems usually requires absorbing boundary conditions to properly truncate the computational domain. Perfectly matched layers (PML) are absorption layers. The PML was introduced by Berenger [2] using artificial electric and magnetic conductivities κ_e and κ_m, respectively, and splitting the electromagnetic field components (split-field formulation). The PML was later shown to be equivalent to a complex coordinate stretching of the coordinate space (coordinate stretching formulation, [3]) and to the uniaxial Maxwellian PML formulation [15].

Using the uniaxial PML formulation the original form of Maxwell's equations is retained. That means, we could easily implement the PML into an existing code. A complex permittivity $[\epsilon]$ and a complex permeability $[\mu]$ diagonal tensor are introduced (see (23), (28), and (29)), resulting in a reflection-free interface between the computational area and the lossy PML region:

$$[\epsilon] = (\epsilon)[\Lambda^{(\epsilon)}], \quad [\mu] = (\mu)[\Lambda^{(\mu)}] \tag{26}$$

with

$$(\epsilon) = \mathrm{diag}(\epsilon_x, \epsilon_y, \epsilon_z), \quad (\mu) = \mathrm{diag}(\mu_x, \mu_y, \mu_z). \tag{27}$$

$[\Lambda^{(\epsilon)}]$ and $[\Lambda^{(\mu)}]$ are defined for a PML in x-, y-, or z-direction in the following way ($\nu \in \{\epsilon, \mu\}$):

$$[\Lambda^{(\nu)}] = \left\{ \begin{array}{l} [\Lambda^{(\nu)}]_x = \mathrm{diag}(\frac{1}{\lambda_\nu}, \lambda_\nu, \lambda_\nu) \\ [\Lambda^{(\nu)}]_y = \mathrm{diag}(\lambda_\nu, \frac{1}{\lambda_\nu}, \lambda_\nu) \\ [\Lambda^{(\nu)}]_z = \mathrm{diag}(\lambda_\nu, \lambda_\nu, \frac{1}{\lambda_\nu}) \end{array} \right\} \quad \text{with} \quad \lambda_\nu = 1 - \jmath\frac{\kappa_\nu}{\nu_0\omega}. \tag{28}$$

That means, we get for an overlapping region in x-, y-, and z-direction:

$$[\epsilon] = (\epsilon)[\Lambda^{(\epsilon)}]_x[\Lambda^{(\epsilon)}]_y[\Lambda^{(\epsilon)}]_z \quad \text{and} \quad [\mu] = (\mu)[\Lambda^{(\mu)}]_x[\Lambda^{(\mu)}]_y[\Lambda^{(\mu)}]_z. \tag{29}$$

The quantities ϵ_0 and μ_0 denote the permittivity and the permeability for a vacuum, κ_ϵ and κ_μ the electric and magnetic (introduced for PML) conductivity, respectively. The lossfree and the lossy case are special variants of (28).

The conductivities have to fulfill the relation

$$\frac{\kappa_\epsilon}{\epsilon_0} = \frac{\kappa_\mu}{\mu_0}. \tag{30}$$

There is always an electric or magnetic wall (see (25)) behind the PML. On the one hand, the PML allows computing the leakage due to radiation effects, on the other hand, the PML can be used to suppress the influence of the boundary on the electric behavior of the structure.

4 Maxwellian Grid Equations

Maxwellian grid equations are formulated for staggered nonequidistant rectangular grids [1, 20, 13] and for tetrahedral nets with corresponding dual Voronoi cells using the Finite Integration Technique with lowest order integration formulae:

$$\oint_{\partial\Omega} \vec{f} \cdot d\vec{s} \approx \sum(\pm f_i s_i), \quad \int_{\Omega} \vec{f} \cdot d\vec{\Omega} \approx f\Omega. \tag{31}$$

4.1 Staggered Nonequidistant Rectangular Grids

The use of rectangular grids is the standard approach. In general, it is very well adapted to planar microwave structures, since most circuits have a basically rectangular geometry. Using (31) Eqs. (21,22) are transformed into a set of grid equations:

$$A^T D_{s/\mu} \vec{b} = \jmath\omega\epsilon_0\mu_0 D_{A_\epsilon} \vec{e}, \qquad B D_{A_\epsilon} \vec{e} = 0, \tag{32}$$

$$A D_s \vec{e} = -\jmath\omega D_A \vec{b}, \qquad \tilde{B} D_A \vec{b} = 0. \tag{33}$$

The vectors $\vec{e}$ and $\vec{b}$ contain the components of the electric field intensity and the magnetic flux density of the elementary cells, respectively. The diagonal matrices $D_{s/\mu}$, D_{A_ϵ}, D_s, and D_A contain the information on cell dimension and material. A , B, and $\tilde{B}$ represent the integrals. A is a singular matrix. B and $\tilde{B}$ are rectangular matrices. A, B, and $\tilde{B}$ are sparse and contain the values $1, -1$, and 0 only. An explicit derivation and a discussion of the properties of (32) and (33) can be found in [12].

By eliminating the components of the magnetic flux density from the two equations on the left-hand sides of (32) and (33), we obtain the system of linear algebraic equations

$$(A^T D_{s/\mu} D_A^{-1} A D_s - k_0^2 D_{A_\epsilon})\vec{e} = 0, \quad k_0 = \omega\sqrt{\epsilon_0\mu_0}, \tag{34}$$

which have to be solved using the boundary conditions (13) and (25), possibly supplemented by PML. k_0 denotes the wavenumber in vacuum.

4.2 Tetrahedral Grids and Voronoi Cells

Using rectangular grids a mesh refinement in one point results in an accumulation of small elementary cells in all coordinate directions, although the refinement is needed only in inner regions. In addition, rectangular grids are not well suited for treatment of curved and non-rectangular structures. A finite-volume method, which uses tetrahedral nets with corresponding Voronoi cells for the three-dimensional boundary value problem, reduces the number of elementary cells by local grid refinement and improves the description of curved structures. The primary grid is formed by tetrahedra and the dual grid by the corresponding Voronoi cells [10].

We consider a tetrahedron $ABCD$ with the internal edge AB (see Fig. 2) and the neighbouring elements, which share the edge AB with it. The electric field intensity components are located at the centers of the edges of the tetrahedra, and the magnetic flux density components are normal to the circumcenters of the triangular faces. The Voronoi cells are polytopes. We use the notations given in Table 1 with $X, Y, Z, W \in \{A, B, C, D\}$, where X, Y, Z, W are different from each other, in order to develop the grid equations for tetrahedral nets. E_{XY} and B_{XYZ} satisfy

$$\begin{aligned} E_{XY} &= -E_{YX}, \\ B_{XYZ} &= B_{YZX} = B_{ZXY} = -B_{YXZ} = -B_{XZY} = -B_{ZYX}, \end{aligned} \tag{35}$$

respectively. The PML boundary conditions are not implemented for tetrahedral grids, i.e. one has (see (26)-(28)),

$$\mu_x = \mu_y = \mu_z = \mu_{XYZW}, \quad \epsilon_x = \epsilon_y = \epsilon_z = \epsilon_{XYZW}. \tag{36}$$

Using a finite volume approach with the lowest-order integration formulae (31), Eqs. (21) and (22) are transformed into a set of grid equations.

Table 1: Notations

X, Y, Z, W	nodes	l_{XY}	distance of X to Y
XY	edge between X and Y	l^W_{XYZ}	distance of T_{XYZW} to XYZ
XYZ	triangle	d^Z_{XY}	distance of S_{XYZ} to XY
$XYZW$	tetrahedron	a_{XYZ}	area of XYZ
S_{XY}	center of XY	μ_{XYZW}	permeability in $XYZW$
S_{XYZ}	circumcenter of XYZ	ϵ_{XYZW}	permittivity in $XYZW$
T_{XYZW}	circumcenter of $XYZW$		
E_{XY}	magnitude of the electric field on S_{XY}		
B_{XYZ}	magnitude of the magnetic flux density on S_{XYZ}		

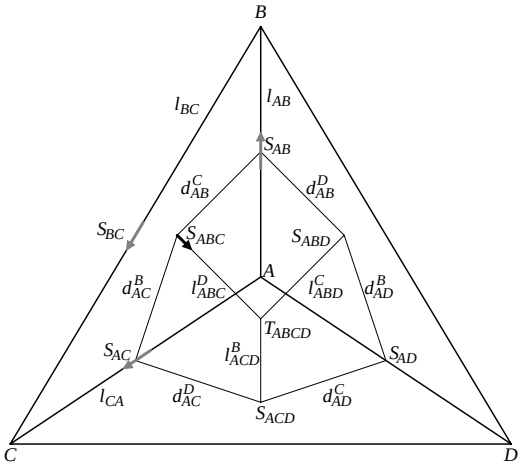

Figure 2: Tetrahedron with partial areas of the Voronoi cell faces related to node A

Taking into account the constitutive relations (23) the first equation of (21) is discretized on the dual grid. The internal edge AB is orthogonal to the corresponding Voronoi cell face over which we have to integrate (see Fig. 2). The closed integration path $\partial\Omega$ (see (21) and (31)) consists of the edges with length $s_i = l^W_{XYZ}$, and is the polygon around the periphery of the mentioned Voronoi cell face. The vertices of the polygon are the circumcenters of the tetrahedra which share the edge AB with the tetrahedron $ABCD$. $f_i = B_{XYZ}$ denotes the function values on S_{XYZ}. Ω is the area of the Voronoi cell face. $f = E_{AB}$ denotes the function value on the center S_{AB}. Thus, the discretized equation takes the form:

$$\begin{aligned} &\textstyle\sum_{CD} \frac{1}{\mu_{ABCD}} \left[l^D_{ABC}\, B_{ABC} + l^C_{ABD}\, B_{ABD} \right] = \\ &\jmath\omega \left[\textstyle\sum_{CD} \frac{1}{2} \epsilon_{ABCD} \left(d^C_{AB}\, l^D_{ABC} + d^D_{AB}\, l^C_{ABD} \right) \right] E_{AB} \end{aligned} \tag{37}$$

where the sum is over those tetrahedra $ABCD$ which share the edge AB.

The first equation of (22) is discretized using (31) on the primary grid. We have to integrate over the triangle ABC. This yields the following form:

$$l_{AB}\, E_{AB} + l_{BC}\, E_{BC} + l_{CA}\, E_{CA} = -\jmath\omega a_{ABC}\, B_{ABC}. \tag{38}$$

Now we address the first of the surface integrals (second equation of (21)) reverting to the dual grid. Here, $\cup\Omega$ is a closed surface with an interior volume. The discretization formula (39), with a form similar to the right-hand side of (37) is obtained, except for the additional outer summation taken over all the nodes B neighboring A (in the primary grid). For our final integral equation (second equation of (22)) the primary grid is used again, but now the integration is over the surface of the tetrahedron $ABCD$. As a consequence, the discretized form (40) can

be deduced:

$$\sum_B \left(\left[\sum_{CD} \frac{1}{2} \epsilon_{ABCD} \left(d^C_{AB}\, l^D_{ABC} + d^D_{AB}\, l^C_{ABD} \right) \right] E_{AB} \right) = 0, \tag{39}$$

$$-a_{ABC}\, B_{ABC} - a_{ACD}\, B_{ACD} + a_{ABD}\, B_{ABD} + a_{BCD}\, B_{BCD} = 0. \tag{40}$$

Substituting the components of the magnetic flux density in (37), (38) the number of unknowns in this system can be reduced by a factor of two:

$$\begin{aligned} &\textstyle\sum_{CD} \frac{1}{\mu_{ABCD}} \left[\left(\frac{l^D_{ABC}}{a_{ABC}} + \frac{l^C_{ABD}}{a_{ABD}} \right) l_{AB}\, E_{AB} + \frac{l^D_{ABC}\, l_{BC}}{a_{ABC}}\, E_{BC} + \right. \\ &\left. + \frac{l^D_{ABC}\, l_{CA}}{a_{ABC}}\, E_{CA} + \frac{l^C_{ABD}\, l_{BD}}{a_{ABD}}\, E_{BD} + \frac{l^C_{ABD}\, l_{DA}}{a_{ABD}}\, E_{DA} \right] = \\ &= \textstyle\frac{\omega^2}{2} \left[\sum_{CD} \epsilon_{ABCD} \left(d^C_{AB}\, l^D_{ABC} + d^D_{AB}\, l^C_{ABD} \right) \right] E_{AB}. \end{aligned} \tag{41}$$

Here, summation is taken over these tetrahedra $ABCD$, which possess the common edge AB.

The method requires a triangulation of the domain in tetrahedra. Thus, triangulation algorithms and grid management are of major importance in the numerical simulation.

Using the grid management interface of the software package pdelib [7], the meshing algorithm COG [18], [17] has been applied.

Based on the octree decomposition technique the software package COG for grid generation and geometry description allows to generate tetrahedral Delaunay meshes [8] with local and anisotropic refinement for arbitrary geometries. A tetrahedral triangulation is roughly spoken a Delaunay triangulation if the circumsphere of each tetrahedron does not contain any vertices of the grid. COG generates -regardless rounding errors - accurate representations of vertices, edges and planar areas at the inner material interfaces and the boundaries of the structures for triangular and rectangular geometries and for geometries which results from its by coordinate transformations. Near curved boundaries special coordinate systems are used which are adapted at a sufficiently large distance to the usual cartesian coordinate system.

Especially, if the circumcenter of a tetrahedron is located within the tetrahedron, we have a clear physical interpretation. The restriction that the circumcenter of a tetrahedron is located within the tetrahedron can not fulfilled in general by a mesh generator. Thus, it can be that the circumcenter of any tetrahedron of the generated Delaunay triangulation is located outside of the tetrahedron, but COG avoids the case that this will be for tetrahedra which are located at inner material interfaces and boundaries. There are no negative distances between two circumcenters. Thus, apart from the physical interpretation the deduced grid equations can be applied using the mentioned properties of COG.

As an example we have simulated a junction of a microstrip line with a coaxial line (see Figs. 3, 4, 5). The structure is symmetric. Thus, only the right half is

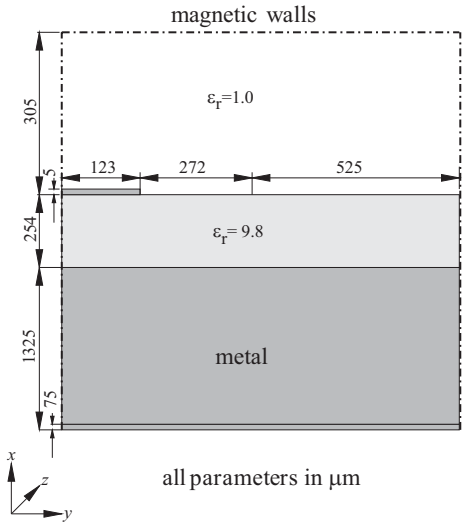

Figure 3: xy-plane

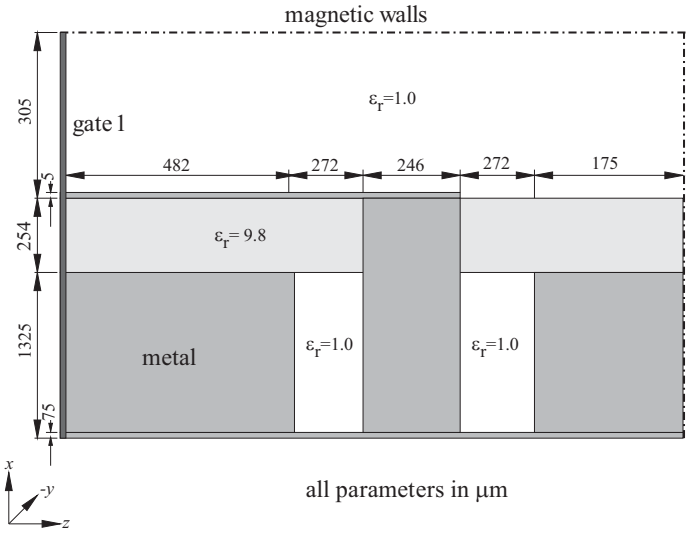

Figure 4: xz-plane

discretized.

For comparison the structure is subdivided in nonequidistant rectangular three-dimensional elementary cells on the one hand and in tetrahedra on the other hand. In case of rectangular grids, the order of the system of linear algebraic equations (see section 6), which corresponds to the boundary value problem (see section 3), is $n = 3n_x n_y n_z = 163\,944$. $n_x n_y n_z$ is the number of cells of the structure which is assumed to be a parallelepiped. We need a high mesh refinement near the microstrip and the coaxial line which results in an accumulation of elementary cells in all coordinate directions even though the refinement is not necessary in order to approximate the solution with the required accuracy.

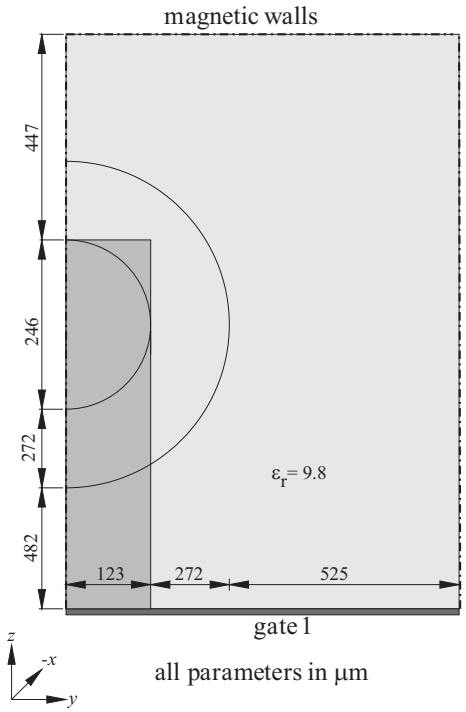

Figure 5: yz-plane

The tetrahedral grid consists of $n_n = 11\,368$ nodes, $n_t = 58\,742$ tetrahedra, and $n_p = 11\,446$ peripheral cell faces. The order of the corresponding system of linear algebraic equations is less than the number of edges:

$$n = n_n + n_t + n_p/2 - 1 = 75\,832. \tag{42}$$

The disadvantage of rectangular grids, the accumulation of elementary cells in all coordinate directions, is avoided here. Curved boundaries are better approximated.

5 Eigenvalue Problem Including PML

For the eigenvalue problem, we refer to the rectangular grid [4].

The transverse electric mode fields (see (24)) at the ports of the three-dimensional structure, which is discretized by means of tetrahedral grids, are computed interpolating the results of the rectangular discretization.

The field distribution at the ports is computed assuming longitudinal homogeneity for the transmission line structure. Thus, any field can be expanded into a sum of so-called modal fields which vary exponentially in the longitudinal direction:

$$\vec{E}(x, y, z \pm 2h) = \vec{E}(x, y, z) e^{\mp \jmath k_z 2h}. \tag{43}$$

k_z is the propagation constant. $2h$ is the length of an elementary cell in z-direction. We consider the field components in three consecutive elementary cells. The elec-

tric field components of the vector $\vec{e}$ (see (34)) $E_{x_{i,j,k+1}}$, $E_{x_{i,j,k-1}}$, $E_{y_{i,j,k+1}}$, $E_{y_{i,j,k-1}}$, $E_{z_{i,j,k-1}}$, $E_{z_{i+1,j,k-1}}$, and $E_{z_{i,j+1,k-1}}$ are expressed by the values of cell k using ansatz (43). The longitudinal electric field components E_z can be eliminated by means of the electric-field divergence equation $BD_{A_\epsilon}\vec{e} = 0$ (see (32)). Thus, we get an eigenvalue problem for the transverse electric fields $\vec{y} = \vec{E}_{t,l}(z_p),\ l = 1(1)m^{(p)}$, (see (24)) on the transmission line region:

$$G\vec{y} = \gamma\vec{y},\ \gamma = e^{-\jmath k_z 2h} + e^{+\jmath k_z 2h} - 2 = -4\sin^2(hk_z). \tag{44}$$

The problem of the transmission line region is reduced to a two-dimensional problem. A detailed derivation of the eigenvalue problem can be found in [12], [11]. The eigenvalue problem has to be solved for each port $z_p,\ p = 1(1)\bar{p}$, (see (1)). The sparse matrix G is general complex. The order of G is $n = 2n_x n_y - n_b$. $n_x n_y$ is the number of elementary cells at the port. The size n_b depends on the number of cells with perfectly conducting material. The solutions of the eigenvalue problem correspond to the propagation constants of the modes. Using a conformal mapping it can be shown that the eigenvalues corresponding to the few interesting modes of smallest attenuation are located in a region bounded by two parabolas. The modes are found solving a controlled sequence of eigenvalue problems of modified matrices [9] applying the invert mode of the Arnoldi iteration with shifts.

The m_s (see (1)) eigenvectors (see (13)) determine the number of right-hand sides of the system of linear algebraic equations (see (48)).

The PML influences the mode spectrum. The absorption inside the PML operates through conductive losses, so that an exponential decay of the fields inside the PML is obtained. The PML achieves a refectionless absorption if the mesh discretization size goes to zero. Caused by the finite mesh size in the finite simulation domain spurious modes are generated due to the electric and magnetic walls behind the absorbing layers. The PML shifts these modes inside the region of propagating modes. We want to distinguish the spurious modes from the desired ones. As a result of our numerical calculations we found that examination of the eigenfunctions provides a useful criterion to select the modes of interest. While the field of guided modes is concentrated around the waveguide structure, the parasitic box modes exhibit a strong field accumulation inside the PML area. Thus, modes that are related to the PML boundary can be detected, using the PPP criterion (Power Part in PML) which is based on the comparison between the power concentration inside the PML region to the whole computational domain [19].

This method, developed initially for a reliable calculation of all interesting complex eigenvalues of microwave structures, was expanded then to meet the special requirements of optoelectronic structure calculations. Relatively large cross sections and highest frequencies (i.e., small wavelengths) yield increased dimensions for the eigenvalue problems. Using the results of a coarse grid calculation within the final fine grid reduces the numerical efforts significantly. A laser application can be found in [9]. A self aligned stripe (SAS) laser with a discretized large cross section of (4050×7750) nm is investigated there. Thin layers of 100 nm with complex material

properties have to be taken into account. The frequency is fixed to $300 * 10^{12}$ Hz, which corresponds to a vacuum wavelengths of 1000 nm. A graded mesh of 121 times 127 elementary cells, including 10-cell PML regions, is used as a coarse grid in order to find approximately the location of the guided mode. A sequence of 84 eigenvalue problems have been used to cover the long small region in the complex plane. The circle that contains the guided mode is known after this step. A graded mesh of 283 times 345 elementary cells, including 10-cell PML regions, is used as a fine grid in order to find the accurate value of the guided mode in the reduced region. The computational time is reduced by a factor of 10 using a coarse and a fine grid.

The use of two levels of parallelization results in an additional speedup in terms of computation time.

6 Systems of Linear Algebraic Equations Including PML

All boundary conditions are known after the computation of the eigen mode problem, and the systems of linear algebraic equations can be solved.

Besides the locations and values of the entries, the matrix representations of (37) - (41) have the same structure as (32) - (34). Thus, we refer to (34) for the solution of the linear algebraic equations.

Multiplying (34) by $D_s^{1/2}$ yields a symmetric form of linear algebraic equations:

$$\bar{A}\vec{x} = 0, \quad \bar{A} = (D_s^{1/2} A^T D_{s/\mu} D_A^{-1} A D_s^{1/2} - k_0^2 D_{A_\epsilon}) \tag{45}$$

with $\vec{x} = D_s^{1/2}\vec{e}$. Moreover, the gradient of the electric field divergence

$$[\epsilon]\nabla([\epsilon]^{-2}\nabla \cdot [\epsilon]\vec{E}) = 0 \tag{46}$$

is used. It can be written as matrix equation

$$\bar{B}\vec{x} = 0, \quad \bar{B} = D_s^{-1/2} D_{A_\epsilon} B^T D_{V_{\epsilon\epsilon}}^{-1} B D_{A_\epsilon} D_s^{-1/2}. \tag{47}$$

The diagonal matrix $D_{V_{\epsilon\epsilon}}$ is a volume matrix for the 8 partial volumes of the dual elementary cell. In case of tetrahedral grids, the gradient of the divergence at an internal point is obtained considering the partial volumes of the appropriate Voronoi cell.

Taking into account the boundary conditions (13) and (25), Eqs. (45) and (47) yield the form $\hat{A}\vec{x} = \vec{b}$ and $\hat{B}\vec{x} = 0$, respectively, and

$$(\hat{A} + \hat{B})\vec{x} = \vec{b}, \;\; \hat{A} + \hat{B} \text{ complex indefinite symmetric}, \tag{48}$$

can be solved faster than $\hat{A}\vec{x} = \vec{b}$.

Independent set orderings [14], Jacobi and SSOR preconditioning using Eisenstat's trick [5] are applied to accelerate the speed of convergence of the used block Krylov subspace method [6, 16] for the system of linear algebraic equations (48) that has to be solved with the same coefficient matrix, but m_s (see (1)) right-hand sides.

The permutations P_i transform the matrices A_i with $A_0 = \hat{A} + \hat{B}$ in the form

$$A_i \quad \longrightarrow \quad P_i A_i P_i^T = \begin{pmatrix} D_i & E_i^T \\ E_i & H_i \end{pmatrix}, \tag{49}$$

where D_i is a diagonal, E_i, and H_i are sparse matrices. Using the factorized form of (49) we get a system of linear equations

$$\begin{pmatrix} I_i & 0 \\ E_i D_i^{-1} & I_i \end{pmatrix} \begin{pmatrix} D_i & E_i^T \\ 0 & H_i - E_i D_i^{-1} E_i^T \end{pmatrix} \begin{pmatrix} \vec{y}_{i,1} \\ \vec{y}_{i,2} \end{pmatrix} = \begin{pmatrix} \vec{c}_{i,1} \\ \vec{c}_{i,2} \end{pmatrix} \tag{50}$$

with $\vec{y}_i = P_i \vec{x}_i = (\vec{y}_{i,1}, \vec{y}_{i,2})^T$ and $\vec{c}_i = P_i \vec{b}_i = (\vec{c}_{i,1}, \vec{c}_{i,2})^T$. The algorithm for solving Eq. (48) is described in the following:

1. Set $A_0 = \hat{A} + \hat{B}$, $\vec{x}_0 = \vec{x}$, $\vec{b}_0 = \vec{b}$
2. Forward substitution: $i = 0, \ldots, lev - 1$
   (a) Compute P_i: $P_i A_i P_i^T$, $\vec{y}_i = P_i \vec{x}_i$, $\vec{c}_i = P_i \vec{b}_i$
   (b) Compute $\vec{x}_{i+1} = \vec{y}_{i,2}$, $\vec{b}_{i+1} = \vec{c}_{i,2} - E_i D_i^{-1} \vec{c}_{i,1}$
   (c) Compute $A_{i+1} = H_i - E_i D_i^{-1} E_i^T$
3. Solve $A_{lev} \vec{x}_{lev} = \vec{b}_{lev}$ for $\vec{x}_{lev}$
4. Backward substitution: $i = lev - 1, \ldots, 0$
   (a) Compute $\vec{y}_{i,2} = \vec{x}_{i+1}$, $\vec{y}_{i,1} = D_i^{-1}(\vec{c}_{i,1} - E_i^T \vec{y}_{i,2})$
   (b) Compute $\vec{x}_i = P_i^T \vec{y}_i$

In comparison to the simple lossy case the number of iterations of Krylov subspace methods increases significantly if the structure contains a PML. In this case, among others, the speed of convergence depends on the relations of the edge lengths in an elementary cell of the nonequidistant rectangular. The best results can be obtained using nearly cubic cells. Moreover, overlapping conditions at the corner regions of the computational domain cause an increase of the magnitude of the corresponding off-diagonal elements in comparison to the diagonal of the coefficient matrix. This deteriorates the properties of the matrix. Thus, overlapping PML should be avoided.

The PML layers, which form the absorbing boundary condition, have a significant influence on computational efforts, which is demonstrated in Table 2 for a quasi-TEM waveguide (in Table 2, ω denotes the relaxation parameter of the Krylov

Table 2: Influence of the PML layers on computational efforts.

	Number of Iteration								
	$\omega = 1.00$			$\omega = 1.30$			$\omega = 1.58$		
f/GHz / Structure	10	50	100	10	50	100	10	50	100
no PML	63	72	127	51	58	104	45	53	91
z-PML	649	647	716	501	518	591	431	452	543
yz-PML	13 912	27 924	32 298	13 501	29 077	45 371	16 457	44 824	104 642
xyz-PML	12 307	44 723	213 358	11 475	55 221	322 155	15 983	111 965	$> 10^6$
xyz-PML (nonov.)	628	591	742	527	479	609	493	436	624

subspace method). A nonequidistant mesh of $27 * 24 * 21$ elementary cells including graded PML regions is used, that means the order of the system of linear algebraic equations is 40 824. The structure is symmetric with respect to the (x, z)-plane. Here, a magnetic wall is used, all other parts of the surface are assumed to be electric walls covered by PML. The longitudinal z-PML region consists of 10 layers, the lateral (x, y)-PML's of 5 layers. The number of iterations also depends on the frequency f and the relaxation parameter ω.

References

[1] Klaus Beilenhoff, Wolfgang Heinrich, and Hans L. Hartnagel. Improved finite-difference formulation in frequency domain for three-dimensional scattering problems. *IEEE Transactions on Microwave Theory and Techniques*, 40, No. 3:540–546, 1992.

[2] J.P. Berenger. A perfectly matched layer for the absorption of electromagnetic waves. *J. Comput. Phys.*, 114:185–200, 1994.

[3] W.C. Chew and W. Weedon. A 3d perfectly matched medium from modified maxwell's equation with stretched coordinates. *Microwave Opt. Technol. Lett.*, 7:599–604, 1994.

[4] Andreas Christ and Hans L. Hartnagel. Three-dimensional finite-difference method for the analysis of microwave-device embedding. *IEEE Transactions on Microwave Theory and Techniques*, 35:688–696, 1987.

[5] S.C. Eisenstat. Efficient implementation of a class of preconditioned conjagate gradient methods. *SIAM J. Sci. Statist. Comput.*, 2:1–4, 1981.

[6] R.W. Freund and W. Malhotra. A Block-QMR algorithm for non-Hermitian linear systems with multiple right-hand sides. *Linear Algebra and Its Applications*, 254:119–157, 1997.

[7] J. Fuhrmann, H. Langmach, I. Schmelzer, and M. Uhle. Grid management in pdelib: sxgrid. http://www.wias-berlin.de/pdelib/documentation/pdelib-1.14.html, sxgrid.ps, 2001.

[8] P.-L. George and H. Borouchaki. *Delaunay Triangulation and Meshing.* Editions Hermes, Paris, 1998.

[9] Georg Hebermehl, Friedrich-Karl Hübner, Rainer Schlundt, Thorsten Tischler, Horst Zscheile, and Wolfgang Heinrich. Simulation of microwave and semiconductor laser structures including absorbing boundary conditions. In Eberhard Bänsch, editor, *Challenges in Scientific Computing - CISC2002*, volume 35 of *Lecture Notes in Computational Science and Engineering, Springer Verlag*, pages 131–159, 2003.

[10] Georg Hebermehl, Jürgen Schefter, Rainer Schlundt, Thorsten Tischler, Horst Zscheile, and Wolfgang Heinrich. Simulation of microwave circuits and laser structures including PML by means of FIT. *Advances in Radio Science*, 2:107–112, 2004.

[11] Georg Hebermehl, Rainer Schlundt, Horst Zscheile, and Wolfgang Heinrich. Improved numerical solutions for the simulation of monolithic microwave integrated circuits. WIAS Preprint no. 236, Weierstraß-Institut für Angewandte Analysis und Stochastik, http://www.wias-berlin.de/publications/preprints/236/, 1996.

[12] Georg Hebermehl, Rainer Schlundt, Horst Zscheile, and Wolfgang Heinrich. Simulation of monolithic microwave integrated circuits. WIAS Preprint no. 235, Weierstraß-Institut für Angewandte Analysis und Stochastik, http://www.wias-berlin.de/publications/preprints/235/, 1996.

[13] Georg Hebermehl, Rainer Schlundt, Horst Zscheile, and Wolfgang Heinrich. Improved numerical methods for the simulation of microwave circuits. *Surveys on Mathematics for Industry*, 9:117–129, 1999.

[14] Y. Saad. *Iterative Methods for Sparse Linear Systems.* PWS Publishing Company, 1996.

[15] Z. S. Sacks, D. M. Kingsland, R. Lee, and J.-F. Lee. A perfectly matched anisotropic absorber for use as an absorbing boundary condition. *IEEE Transactions on Antennas and Propagation*, 43:1460–1463, 1995.

[16] Rainer Schlundt, Georg Hebermehl, Friedrich-Karl Hübner, Wolfgang Heinrich, and Horst Zscheile. Iterative solution of systems of linear equations in microwave circuits using a block quasi-minimal residual algorithm. In Ursula van Rienen, Michael Günther, and Dirk Hecht, editors, *Scientific Computing in Electrical Engineering*, volume 18 of *Lecture Notes in Computational Science and Engineering, Springer Verlag*, pages 325–333, 2001.

[17] I. Schmelzer. COG. http://www.wias-berlin.de/software/cog/index.html, 2000.

[18] I. Schmelzer. Grid generation and geometry description with COG. In A. Handlovičová, M. Kormorníková, K. Mikula, and D. Ševčovič, editors, *Proceedings of contributed papers and posters, ALGORITM 2000, 15th Conference on Scientific Computing*, pages 399–405, Vysoké Tatry - Podbanské, Slovakia, September 10 - 15, 2000. Slovak University of Technology, Bratislava.

[19] Thorsten Tischler and Wolfgang Heinrich. The perfectly matched layer as lateral boundary in finite-difference transmission-line analysis. *IEEE Transactions on Microwave Theory and Techniques*, 48:2249– 2253, 2000.

[20] T. Weiland. A discretization method for the solution of Maxwell's equations for six-component fields. *Electronics and Communication (AEÜ)*, 31:116–120, 1977.